Energy Reports 8 (2022) 15048–15056

Contents lists available at ScienceDirect

Energy Reports

journal homepage: www.elsevier.com/locate/egyr

Research paper

Flexible carbon cloth-based single-electrode triboelectric nanogenerators with incorporated TiO_2 nanoparticles

Roman Kruchinin [a], Yerzhan Nurmakanov [a], Galymzhan Nauryzbayev [b], Desmond Adair [c], Zhumabay Bakenov [d], Gulnur Kalimuldina [c,*]

[a] School of Engineering and Digital Sciences, Nazarbayev University, Kabanbay Batyr Ave. 53, Nur-Sultan 010000, Kazakhstan
[b] Department of Electrical and Computer Engineering, School of Engineering and Digital Sciences, Nazarbayev University, Kabanbay Batyr Ave. 53, Nur-Sultan 010000, Kazakhstan
[c] Department of Mechanical and Aerospace Engineering, School of Engineering and Digital Sciences, Nazarbayev University, Kabanbay Batyr Ave. 53, Nur-Sultan 010000, Kazakhstan
[d] Department of Chemical and Materials Engineering, School of Engineering and Digital Sciences, Nazarbayev University, Kabanbay Batyr Ave. 53, Nur-Sultan 010000, Kazakhstan

ARTICLE INFO

Article history:
Received 16 August 2022
Received in revised form 31 October 2022
Accepted 5 November 2022
Available online xxxx

Keywords:
Energy harvesting
Mechanical energy
Triboelectric nanogenerator
Self-powered electronics
Carbon cloth
Polydimethylsiloxane

ABSTRACT

Recently, flexible triboelectric nanogenerators (TENGs) have gained significant interest as a promising autonomous technology for harvesting abundant mechanical energy and powering portable electronic devices. In this work, a high-performance flexible single-electrode TENG (SETENG) is presented with a highly conductive carbon cloth (CC) textile electrode and an encapsulating triboelectric material based on polydimethylsiloxane (PDMS). To increase the generation of triboelectric charges, a rough microtextured surface is implemented on the PDMS friction layer through a simple imprint lithography approach. In addition, the output performance of the prepared SETENG device is further improved by incorporating various concentrations of titanium dioxide (TiO_2) nanoparticles. As a result, flexible CC@TiO_2-PDMS SETENGs efficiently converts the mechanical energy into electrical power through continuous contact/separation processes caused by the counter tribo-positive friction objects (i.e., human skin, nylon, and cotton fabrics). It was shown that a sample with 5 wt% TiO_2, CC@5wt%TiO_2-PDMS SETENG, achieves the highest output and a sample of 6 × 2.5 cm^2 area could charge capacitors (0.1, 1, 10 μF) and power 130 LEDs connected in series. Finally, the demonstration of a fully functioning SETENG-powered calculator provides strong evidence of the current maturity of the technology and its excellent potential for self-powered small electronics application.

1. Introduction

Harvesting energy from renewable resources has been considered as one of the effective approaches to fulfill the growing demand for energy and sustainable development. Among many renewable energy sources, mechanical energy is found to be the most widespread and readily available in nature (Dharmasena and Silva, 2019; Zhou et al., 2018). In the era of the Internet of Things (IoT), big data, and the rapid development of small-scale electronic devices, a challenge arises as to the development of a versatile and autonomous power supply technology (Shi et al., 2021; Wang, 2014). The use of traditional energy storage devices for power supply, such as batteries and capacitors, in the plethora of portable devices and sensors, is accompanied by the problem of their recurrent recharging or replacement. An alternative energy source for charging these devices offline is required to cope with these issues.

One of such promising energy sources is a triboelectric nanogenerator (TENG), an energy-harvesting device that converts mechanical energy into electrical energy based on the triboelectric effect and electrostatic induction (Cao et al., 2016; Fan et al., 2012b; McCarty and Whitesides, 2008). The electricity generation occurs during the periodical contact/separation or sliding movements between two surfaces with different electron affinities. Moreover, TENGs are also suitable for harvesting random mechanical energy as their excitation frequency can vary from several Hz to hundreds of Hz (Chen and Wang, 2017). TENG can be used as an energy harvester and a self-powered sensor, applications of which are found in healthcare, weather control, and robotics (Jin et al., 2020; Khandelwal et al., 2020; Wang et al., 2015; Zhang and Wang, 2016). Compared to the piezoelectric, electromagnetic, and thermoelectric generator technologies, the advantages of TENG are that they have a high energy density

* Corresponding author.
E-mail address: gkalimuldina@nu.edu.kz (G. Kalimuldina).

https://doi.org/10.1016/j.egyr.2022.11.049

output, good conversion efficiency, material selection versatility, and low cost (Nie et al., 2019; Wang, 2013). In terms of the operation of a TENG, four fundamental modes (vertical contact-separation mode, lateral sliding mode, single-electrode mode, and the freestanding triboelectric layer mode) define the device design. Typical TENGs have sophisticated structures with a pair of triboelectric materials and two electrodes (Luo and Wang, 2020; Niu et al., 2013; Wang et al., 2013, 2017). However, recently, more work was reported on the single-electrode mode TENG (SETENG) as it has the advantage of being simple in terms of fabrication and assembling, due to the possession of only one electrode and one triboelectric layer (Niu et al., 2014; Wang et al., 2016). In that case, an external object serves as the other triboelectric layer, saving space and enhancing TENG's practical applications.

Although it was reported that TENG could be prepared from any different-in-nature materials (Nurmakanov et al., 2021; Zhang and Olin, 2020), a high-performance TENG is achievable only by a careful selection of an appropriate pair of materials, device design, and, specifically, contact electrification enhancement via chemical and physical modifications (Zhou et al., 2020). The two main parts of TENG are the triboelectrification material and the conductive electrode. For the fabrication of the latter, many conductive materials have been investigated, such as copper, steel, aluminum wires and foils (Nurmakanov et al., 2021; Xie et al., 2019), fibers or fabrics coated with metal, carbonaceous nanoparticles (NPs) (Cui et al., 2018; Xia et al., 2020; Zhou et al., 2019), and conductive polymers (Dudem et al., 2019; Mule et al., 2019). However, the main drawback of these systems is poor durability during mechanical deformations. Moreover, the fabric electrodes, coated with metal, carbonaceous NPs, and conductive polymers, suffer from conductivity deterioration due to the conductive layer's wearing. Therefore, significant efforts have been dedicated to finding alternative conductive materials with higher flexibility and durability for nanogenerator applications. It is envisioned that the electrodes made of textile conductive interlacing fibers can be more promising materials for developing wearable and flexible TENGs. For instance, carbon cloth (CC) made of carbon fibers is flexible, lightweight, mechanically durable, chemically inert, and resistant to corrosion and also possesses a conductivity comparable to that of metals (Mishra et al., 2019; Shi et al., 2020). However, CC has not been thoroughly investigated as an electrode for TENG devices, with only a few studies reporting the applications of CC. Flexible triboelectric nanogenerator (FTENG) composed of PDMS/3D bilayer graphene/CC was demonstrated (Qian et al., 2020) with the maximum values of the peak-to-peak output voltage and current density of 70 V and 9.3 μA cm^{-2}, respectively. Another study reported a novel wearable TENG based on nickel-copper bimetallic hydroxide nanowrinkles grown on a CC electrode (Xia et al., 2020), and this device showed a maximum output power density of 1.323 mW cm^{-2}.

In regard to the second part of a TENG, i.e., triboelectric materials, the choice of a suitable tribo-layer has a decisive role in the final performance of the device. PDMS has been widely studied for TENG applications among other polymers due to its flexibility, hydrophobic properties, and excellent electronegativity, enabling withdrawal charges from other materials (Tantraviwat et al., 2021). However, pure PDMS does not exhibit high triboelectric performance. Therefore, surface nanopatterning, chemical functionalization, and dielectric properties modulation methods allowed achieving higher charge densities (Cheng et al., 2017; Fan et al., 2012a; Kim et al., 2021; Zhang et al., 2014). For example, a considerable increase in the voltage and current outputs was observed when nanofillers were added to the bulk of the PDMS (Kang et al., 2020). The triboelectric charge density is directly related to the capacitance of a triboelectric material. Thus, an increase in the relative material permittivity by introducing nanofillers increases its capacitance and, accordingly, charge density. High-permittivity NPs are believed to enhance the dielectric constants of polymer composite layers through interface polarization. For instance, the triboelectric performance has been shown to be enhanced by incorporating $BaTiO_3$ (Ali et al., 2017; Kang et al., 2020), Al-doped $BaTiO_3$ (Dudem et al., 2018), $CaCu_3Ti_4O_{12}$ (Fang et al., 2018), and TiO_2 nanofillers into the triboelectric layer (Jian et al., 2021; Park et al., 2018). TiO_2 NPs have been intensively investigated as nanofillers to enable high-performance TENGs due to their excellent properties such as a high dielectric constant, chemical stability, nontoxicity, and low cost. For instance, Park et al. defined that not only an increase in the dielectric constant is taking place with the addition of a small amount of TiO_2 NPs, but also an additional mechanism based on the role of oxygen vacancy in TiO_2NPs embedded PDMS. The electron flow can efficiently be trigged via attractive force at the negative tribo-material surface with more induced oxygen vacancies that are electrically positively charged (Park et al., 2018).

Despite the promising results for TENG devices, the fabrication process and their structural design still require a more simplified approach. This is especially essential for developing flexible and wearable devices, since the performance of TENG is highly reliant on the metal, metal/conductive polymer-based electrodes, which will hinder its wearability and durability properties.

To address these challenges, we proposed a facile method to fabricate flexible and high-performance SETENG based on a highly conductive CC electrode and microstructured PDMS triboelectric material. To the best of our knowledge, the application of a flexible CC electrode has not yet been reported for SETENG mechanical energy harvesting devices. Furthermore, excellent SETENG performance was demonstrated under various concentrations of TiO_2 NPs incorporated into the PDMS. The optimal performance with the highest output was achieved for SETENG with 5 wt% TiO_2 NPs (CC@5wt%TiO_2-PDMS SETENG). To be more specific, this SETENG could reach an open-circuit voltage (V_{oc}) and short-circuit current (I_{sc}) of 116 V and 1.42 μA, respectively, and was able to light up 130 green light-emitting diodes (LEDs) connected in series. The impact of an external pressing force and external load resistance on the electrical output characteristics of the CC@5wt%TiO_2-PDMS SETENG were systematically investigated, and the experiments showed that the CC@5wt.%TiO_2-PDMS SETENG could charge external energy storage devices such as a capacitor and successfully operate a calculator.

2. Material and methods

2.1. Materials

PDMS (Sylgard 184, Sigma-Aldrich), TiO_2 nanopowder (particles size < 25 nm, Sigma Aldrich), and CC (thickness: ∼0.5 mm) were used. All the chemicals were of laboratory grade and used as received.

2.2. SETENG fabrication

Fig. 1 shows the schematic diagram of a SETENG fabrication process. The SETENG dimensions were 6 cm in length, 2.5 cm in width and 5 mm in thickness (d_1). First, the Sylgard 184 base and curing agent at a ratio of 10:1 was added and thoroughly mixed with TiO_2NPs (5, 10, 20 wt%). Then, the as-prepared solution was poured onto the rough side of sandpaper and followed by placing a CC electrode. More solution was then poured above the electrode. The fully encapsulated CC electrode was put into a vacuum chamber to remove air bubbles and then into an oven to cure the PDMS at 150 °C for 1.5 h. Finally, the CC@TiO_2-PDMS

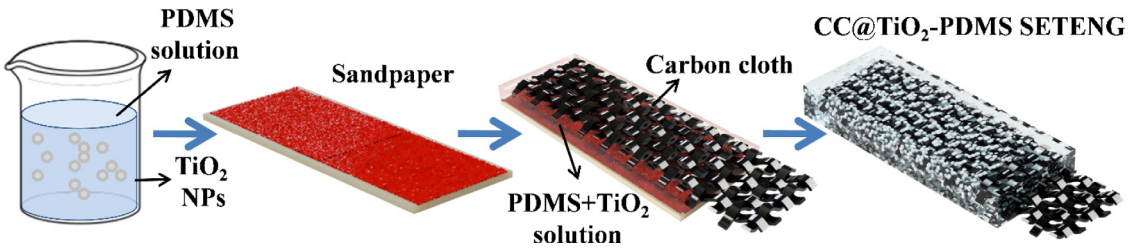

Fig. 1. A schematic fabrication process of CC@TiO_2-PDMS SETENG with a patterned surface.

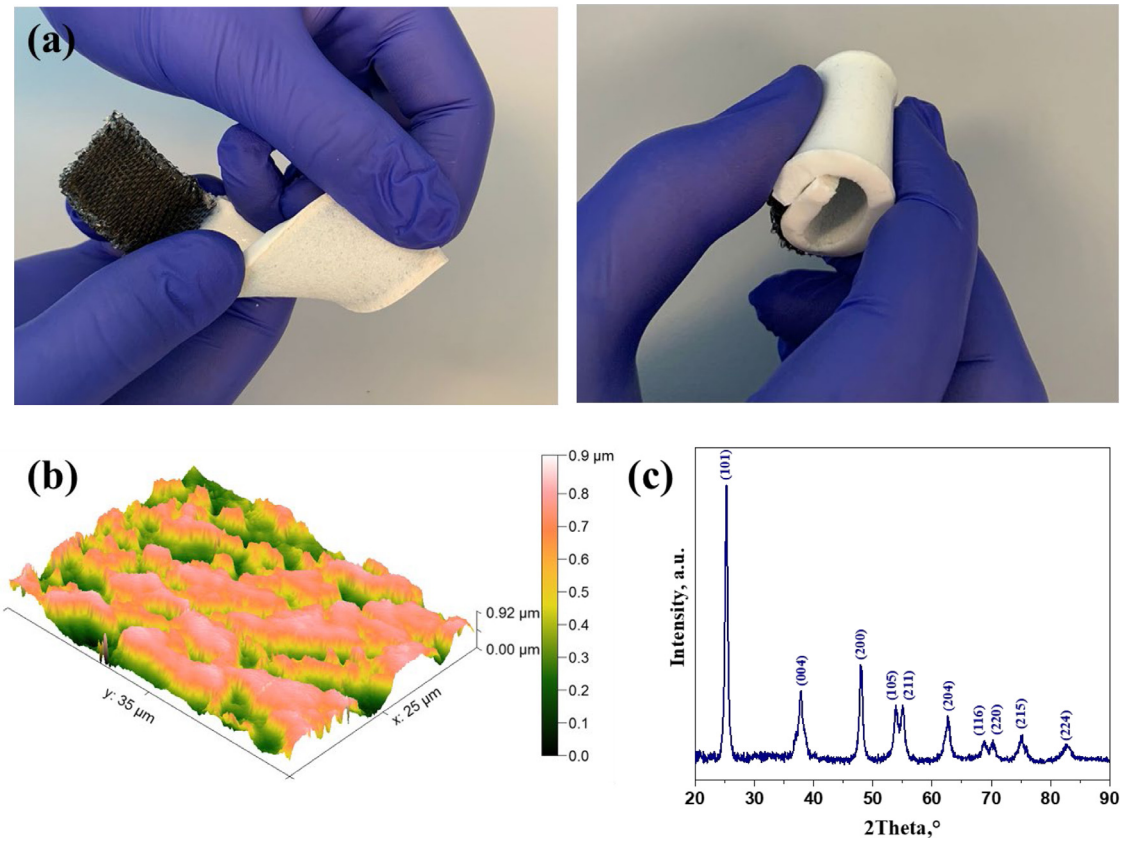

Fig. 2. (a) Images of flexible TENG, (b) 3D AFM image of the patterned surface of CC@5wt%TiO_2-PDMS SETENG, (c) XRD pattern of anatase TiO_2NPs.

SETENG device with the micropatterned triboelectric surface was obtained after being easily peeled off from the sandpaper. The gap distance between CC@TiO_2-PDMS SETENG and cotton fabric (electron donor surface with 1 mm thickness (d_2)) was designed to be 13 mm (d_3).

2.3. SETENG characterization

The field-emission scanning microscope (FE-SEM, Crossbeam 540, Zeiss) and atomic force microscopy (AFM, SmartSPM, AIST-NT) were employed to examine the surface morphology of the prepared CC@TiO_2-PDMS SETENG. The physical structure of TiO_2 NPs was analyzed using X-ray diffraction (XRD, SmartLab, Rigaku). The output voltage and current measurements of CC@TiO_2-PDMS SETENGs were carried out in a vertical contact/separation mode with a single-electrode configuration. The output voltage and current were measured using a digital oscilloscope (Tektronix TDS 2002C) and a low-noise current preamplifier (Stanford Research SR570) combined with the oscilloscope. The linear motor (LinMot E1100) was used to achieve periodic contact/separation movements. The force sensor (Vernier LabQuest Mini) was used to measure the applied force.

3. Results and discussion

Fig. 2a shows the fabricated CC@TiO_2-PDMS SETENG device demonstrating high flexibility during its mechanical bending and rolling. The morphology of the patterned PDMS layer side was studied by AFM as demonstrated in Fig. 2b. The AFM image defines a surface roughness of 206.3 nm. TiO_2 has several structural forms, namely, anatase, rutile, and bookite, and, the structure, electrical and optical properties of TiO_2 change. The crystallinity and structure of the added TiO_2NPs were analyzed by XRD as shown in Fig. 2c. The XRD results confirm that the TiO_2 particles have a typical anatase structure (ICDD 00-001-0562) with a crystallite size of about 18 nm.

The electrical properties of SETENGs were evaluated using the in-house testing device system illustrated in Fig. 3a. A piece of cotton fabric was initially chosen as an electron donor surface when contacted with the PDMS for the single-electrode mode

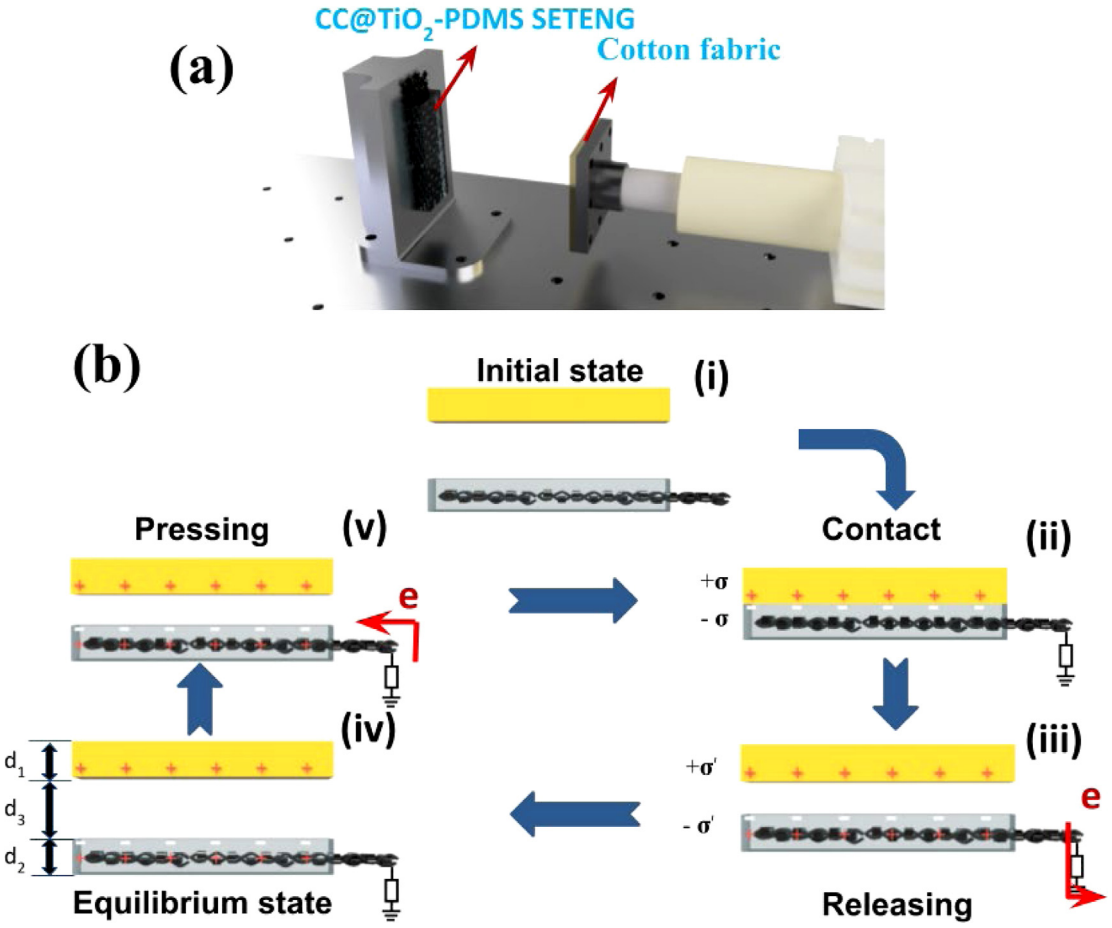

Fig. 3. (a) Schematic illustration of measuring system for typical electric output of fabricated TENGs; and (b) working principle of CC@TiO_2-PDMS SETENG devices operated in a contact/separation mode.

testing. A linear motor implemented periodic contact/separation movements between the cotton fabric and the CC@TiO_2-PDMS SETENGs. Additionally, a force sensor was embodied on a 3D printed frame with a polyethylene terephthalate rectangular plate fixed on a sensor to measure the applied force by the cotton fabric to the PDMS surface. The working mechanism is schematically shown in Fig. 3b, where the generation of electrical outputs occurs during the contact/separation of two different materials with opposite triboelectric tendencies. Initially, there is a gap between the PDMS and cotton fabric surfaces in the absence of an external force and they remain electrically neutral. Once an external force is applied to the TENG pair, the PDMS and cotton fabric surfaces contact with each other.

As a result, the charge transfer leads to the generation of static charges at the surfaces of opposite polarities. According to the material properties, the PDMS-based surface attracts electrons stronger than the cotton fabric. Therefore, the electrons will be injected from the cotton onto the surface of the PDMS, resulting in the cotton fabric becoming positively charged and the PDMS surface becoming negatively charged. Due to the electrostatic effect, the negative charges on the PDMS surface layer will induce positive charges on the CC electrode as the cotton fabric moves away. Thus, free electrons flow from the CC electrode to the ground, and as a result, produce the output signal. When the cotton fabric completely separates from the PDMS layer, the negative charges on the surface of the PDMS layer are fully screened from the induced positive charges on the CC electrode. Therefore, no electrical signal is observed. However, when both PDMS and cotton fabric layers again come in contact, the induced positive charges on the CC decrease. This is mainly attributed to the flow of electrons from the ground to the CC, resulting in a reversed electrical output current signal. Thus, the alternating electrical output can be observed due to the electrons flowing back and forth between CC and the ground under the continuous contacts/separations between the triboelectric materials.

To investigate the effect of TiO_2 NPs on the electrical properties of CC@TiO_2-PDMS SETENG, samples with 5, 10 and 20 wt% TiO_2 NPs were prepared. As shown in Fig. 4a,b, as the weight ratio of TiO_2 NPs increases from 0 (pure PDMS) to 5 wt%, V_{oc} and I_{sc} increase notably from 40 V and 0.42 μA to 116 V and 1.42 μA, respectively. This output improvement is mainly due to the enhancement of the dielectric constant, as shown in **Fig. S1** in the supplementary material (SM), the dielectric constant linearly changes as a function of the anatase TiO_2 NPs embedded PDMS in different weight ratios. The dielectric constant contributed to the charge capacitance at the surface of the composite PDMS layer and cotton fabric intensifying triboelectrification contributed to the enhanced electrical output of the CC@5wt%TiO_2-PDMS SETENG.

However, it is imperative to note that the other modifications of CC@TiO_2-PDMS SETENGs with the TiO_2 NPs content above 5 wt% demonstrated a worse performance. For instance, attained peak-to-peak V_{oc} and I_{sc} were equal to 79.5 V and 0.74 μA for the nanogenerator with 10 wt% of TiO_2NPs. It became obvious that the performance was compromised when the TiO_2 NPs exceeded 5 wt% as TiO_2 NPs are more likely to agglomerate in the PDMS at higher concentrations (**Fig. S2** in SM). Such agglomerations could

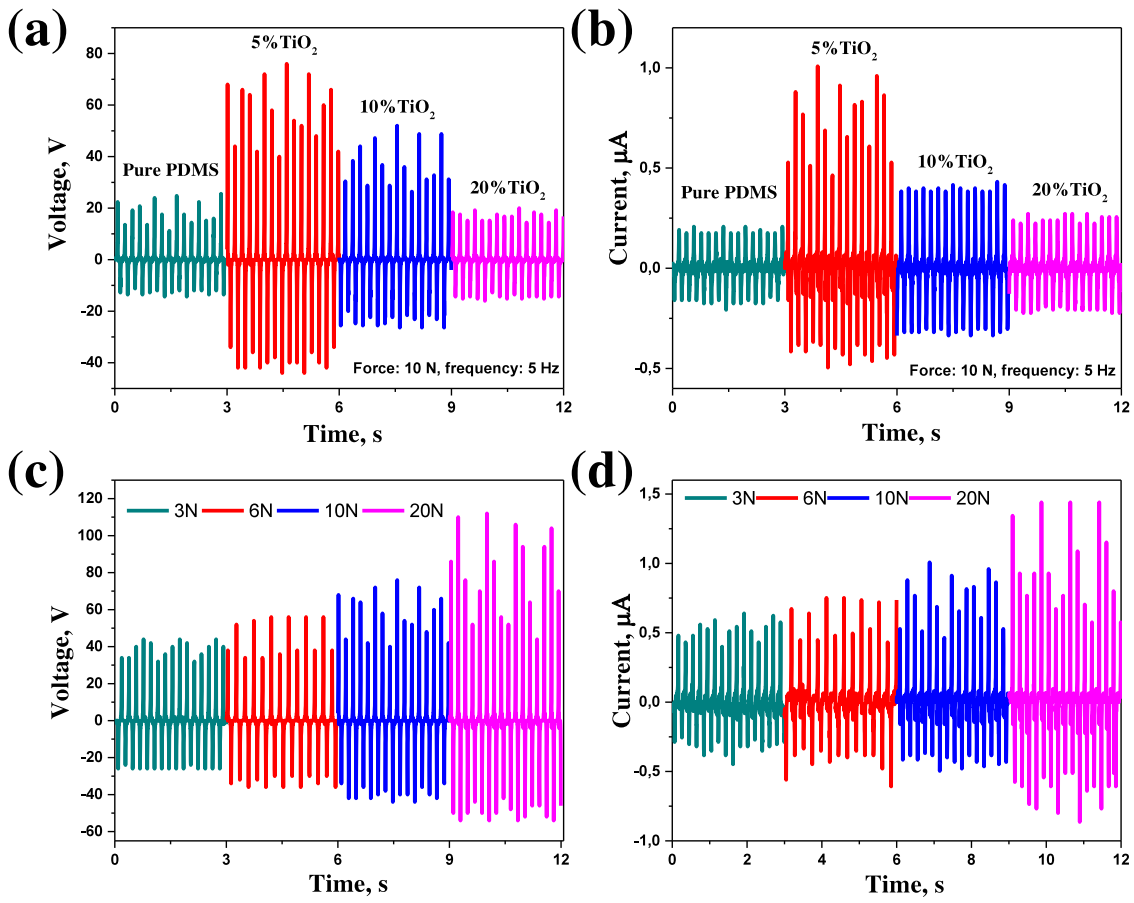

Fig. 4. Output performance of CC@TiO_2-PDMS SETENGs: (a, b) impact of TiO_2 NPs wt% on V_{oc} and I_{sc}, (c), (d) V_{oc} and I_{sc} under various applied external forces for CC@5wt%TiO_2-PDMS SETENG.

form conductive networks favoring leakage current (Zhou et al., 2020).

The effect of an applied force on the electrical properties of the CC@5wt%TiO_2-PDMS SETENG with the best electrical output was also investigated. Fig. 4c and d show the output voltage and current of the CC@5wt%TiO_2-PDMS SETENG under a fixed 5 Hz frequency. When the applied forces increased from 3 to 20 N, the corresponding peak-to-peak values of V_{oc} and I_{sc} also increased from 71.4 V and 0.98 μA to 166.5 V and 2.0 μA, respectively. The growth in V_{oc} and I_{sc} with applied force comes from an increase in the contact area between the PDMS-based surface and the cotton fabric (Min et al., 2021). The visual demonstration has been presented in **Fig. S3** in SM.

The output power of the flexible CC@5wt%TiO_2-PDMS SETENG was evaluated and calculated by connecting various resistances externally (from 1 MΩ to 1 GΩ). The impedance data of the CC@5wt%TiO_2-PDMS SETENG are shown in Fig. 5a, and it can be observed that V_{oc} increases up to 190 V when the resistance value increases from 1 MΩ to 610 MΩ and afterwards V_{oc} decreases, while the output current follows the reverse trend. The corresponding output power of the CC@5wt%TiO_2-PDMS SETENG was also plotted as a function of the external resistance (Fig. 5b). The results reveal that the output power density increases at a low resistance and decreases at a higher resistance. The maximum value exhibits 3.6 μWcm^{-2} at an external resistance of 520 MΩ. The maximum power transfer in alternating current (AC) sources occurs when the impedance of the source and the load match. The impedance of the SETENG is large (in MΩ), and if the impedance of the load is much larger or smaller than the source impedance, the power transfer is degraded. To get the maximum power output of the SETENG, it is recommended to match it with a load with a similar impedance.

The mechanical endurance and long-term working stability tests were carried out to investigate the sustainability and durability of the CC@5wt%TiO_2-PDMS SETENG. In Fig. 5c, the output voltage response of the corresponding device was measured continuously for 9000 cycles. The output voltage of the device remained consistent at about 100 V in response to an external continuous compressive force of 10 N. The results revealed the outstanding stability of the prepared CC@5wt%TiO_2-PDMS SETENG without any degradation of the electrical output.

Moreover, the CC@5wt%TiO_2-PDMS SETENG was further tested in contact with other textile fabrics such as polyester, nylon and human skin to confirm its potential for application as a wearable device as illustrated in Fig. 5d. The variations in V_{oc} coincide well with the reported tribo-series list, where two materials with a significant difference in series, depending on their relative triboelectric charge attracting/receiving characteristics to produce higher output (Khandelwal et al., 2021). For instance, in the current work, the CC@5%TiO_2-PDMS SETENG in contact with the human skin generates 130 V as tribo-negative PDMS and tribo-positive human skin have distinctly opposing triboelectric properties. The obtained data demonstrate that the practical application of the CC@5%TiO_2-PDMS SETENG is possible as a power source for wearable electronic devices and smart clothes through harvesting energy in contact/separation with various surrounding surfaces.

Since electronic devices are powered by a direct current (DC) source, the practical applications of the CC@5wt%TiO_2-PDMS SETENG were demonstrated by rectifying the generated AC into

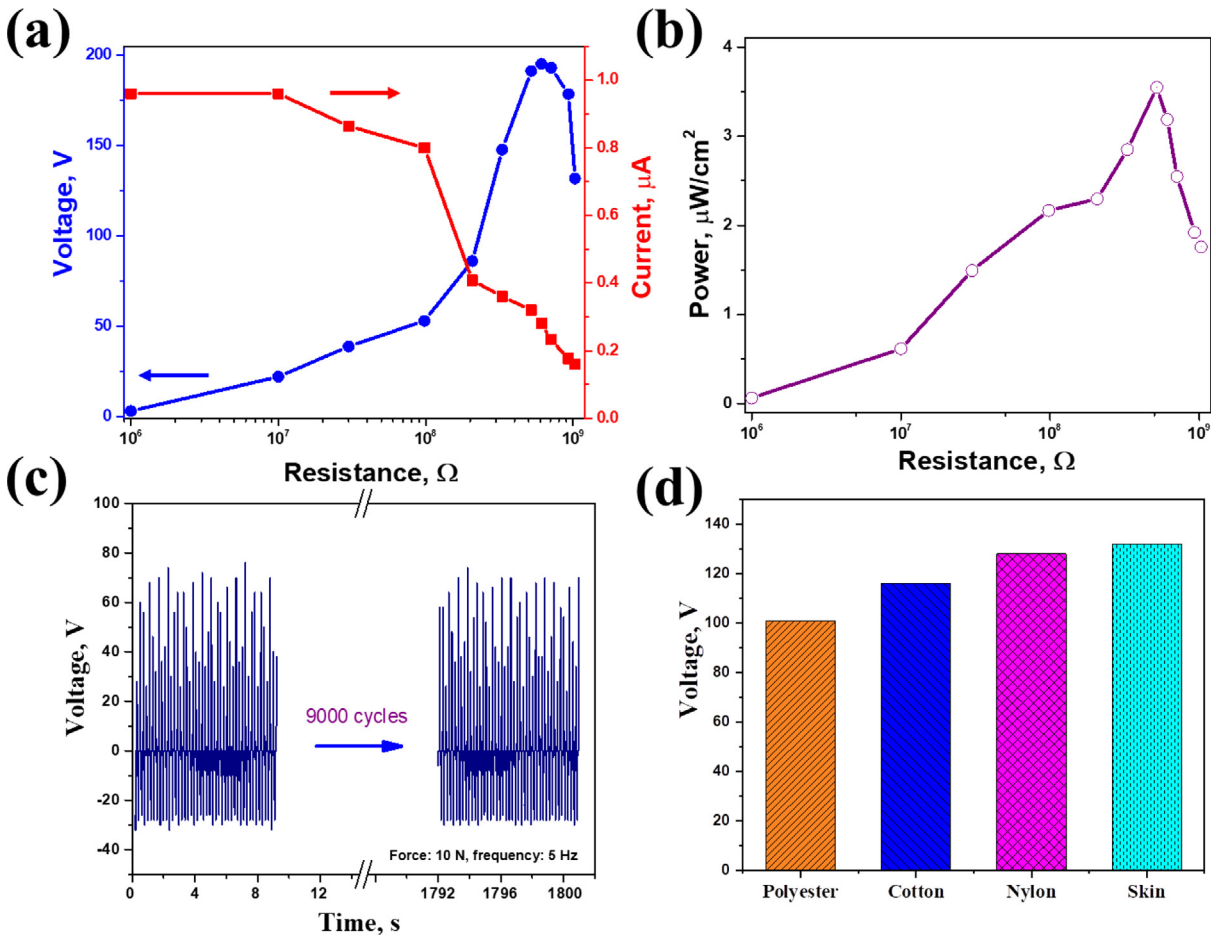

Fig. 5. Electrical characterization of CC@5wt.%TiO_2-PDMS SETENG: (a) dependence of output V_{oc} and I_{sc}, (b) output power density on the value of external load resistance, (c) output V_{oc} of device with continuous application of cycled compressive force for 9000 cycles, (d) output V_{oc} of device interacting with different textile fabrics and human skin.

DC. The equivalent electrical circuit, consisting of a conventional diode bridge rectifier, was used to achieve DC as shown in Fig. 6a. The rectified output of the CC@5wt%TiO_2-PDMS SETENG, at a load of 10 N and frequency of 5 Hz, exhibited all-positive featured peaks of 45 V (Fig. 6b). The ability to charge a capacitor by the CC@5wt%TiO_2-PDMS SETENG is demonstrated in Fig. 6c, where the charge–discharge curve profile for a 1-μF capacitor shows successful charging from 0 to 30 V within 300 s. The mechanical energy storage in a capacitor was further studied for the capacitors of 0.1, 1 and 10 μF, as shown in Fig. 6d.

In addition, the CC@5%TiO_2-PDMS SETENG was attached to clothes to examine their real-life electrical output performances. Fig. 7a and b illustrate the experiments, where corresponding SETENG was placed under the arm of a sweater and a foot heel. When the device was attached under the arm, the generated peak-to-peak voltage was about 10 V, whereas in the case of SETENG placed under the foot heel, it exhibited 45 V. The output signal generated by walking is higher than that from the arm motions. It confirms that SETENGs set under the foot heel experience higher impact force, hence providing an effective contact surface between the device and paper tissue on a floor. In Fig. 7c, we present an image, where the CC@5wt%TiO_2-PDMS SETENG by hand tapping directly lights 130 LEDs connected in series (please also see a video in the SI). The application of flexible CC@5wt%TiO_2-PDMS SETENG for self-charging systems was confirmed when a 220-μF capacitor with the stored energy powered a calculator (Fig. 7d) (please also see a video in the SI).

Table 1 compares various SETENGs based on PDMS material with additives. Since not many works were reported on SETENG modes of triboelectric materials, we can confirm that CC@5wt%TiO_2-PDMS SETENG shows competitive results considering easy fabrication and durable electrode (CC) considerations. SETENG devices are particularly suitable to be integrated into wearable devices as the connections and wiring are required to be developed for only a single electrode.

4. Conclusions

In conclusion, this work demonstrated the preparation of a flexible single electrode SETENG as an efficient mechanical energy harvesting device. Highly conductive CC and PDMS with nanofillers were used as electrode and tribo-negative material, respectively. The surface micro-patterning of the PDMS, implemented by a simple imprint lithography, was used to increase the charge density at the contact surface. Moreover, adding specific amounts of TiO_2 NPs further enhanced the dielectric properties of PDMS. Both surface microstructuring and incorporation of NPs improved the SETENG performance. Particularly, the addition of 5 wt% TiO_2 NPs resulted in a significant increase in peak-to-peak V_{oc} and I_{sc} of 116 V and 1.42 μA, respectively, which stands for a 2.9-fold and 3.4-fold growth in the corresponding metrics. Finally, the produced flexible CC@5wt%TiO_2-PDMS SETENG device was proven to be able to power 130 LEDs connected in series and charge a 1-μF capacitor within 300 s Last but not least, the SETENG-enabled calculator was also demonstrated to highlight the huge potential of such nanogenerators for self-powered wearable electronics.

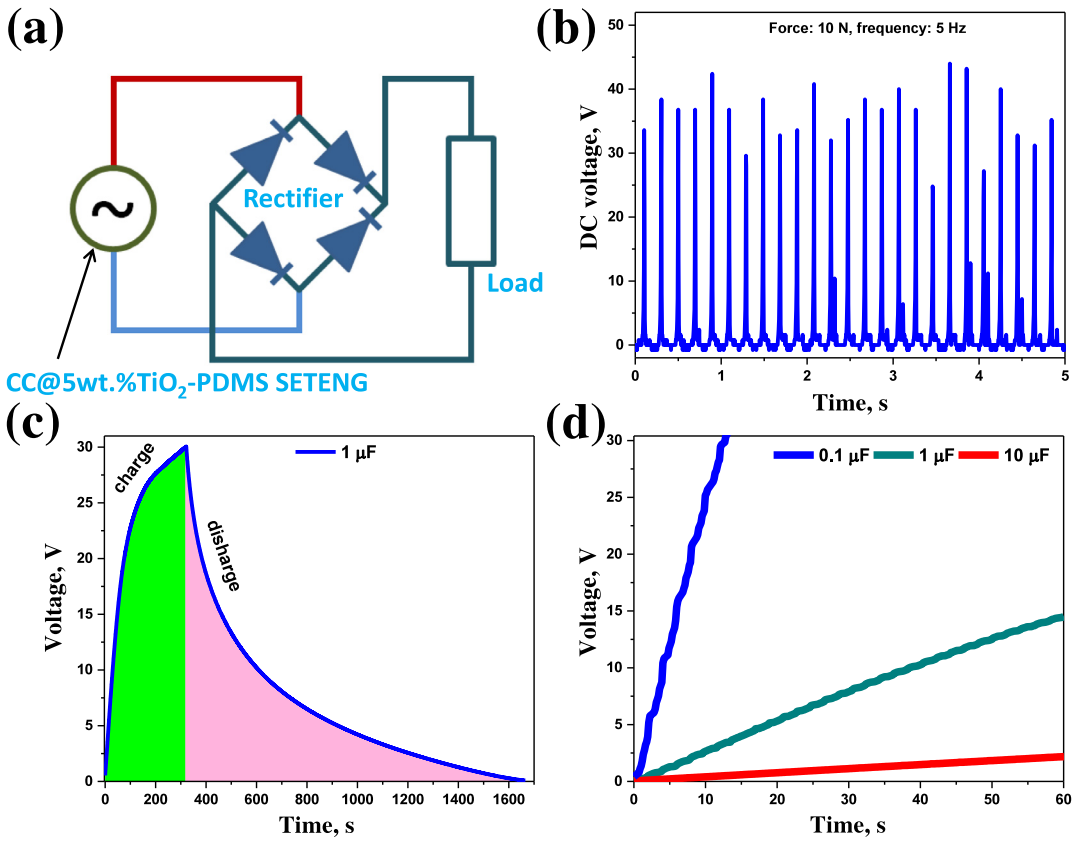

Fig. 6. (a) A circuit for rectifying AC electrical output, (b) a rectified output voltage from CC@5wt%TiO_2-PDMS SETENG, (c) charge–discharge profile of 1μF capacitor, (d) charging curves of 0.1, 1 and 10μF capacitors charged by CC@5wt.%TiO_2-PDMS SETENG.

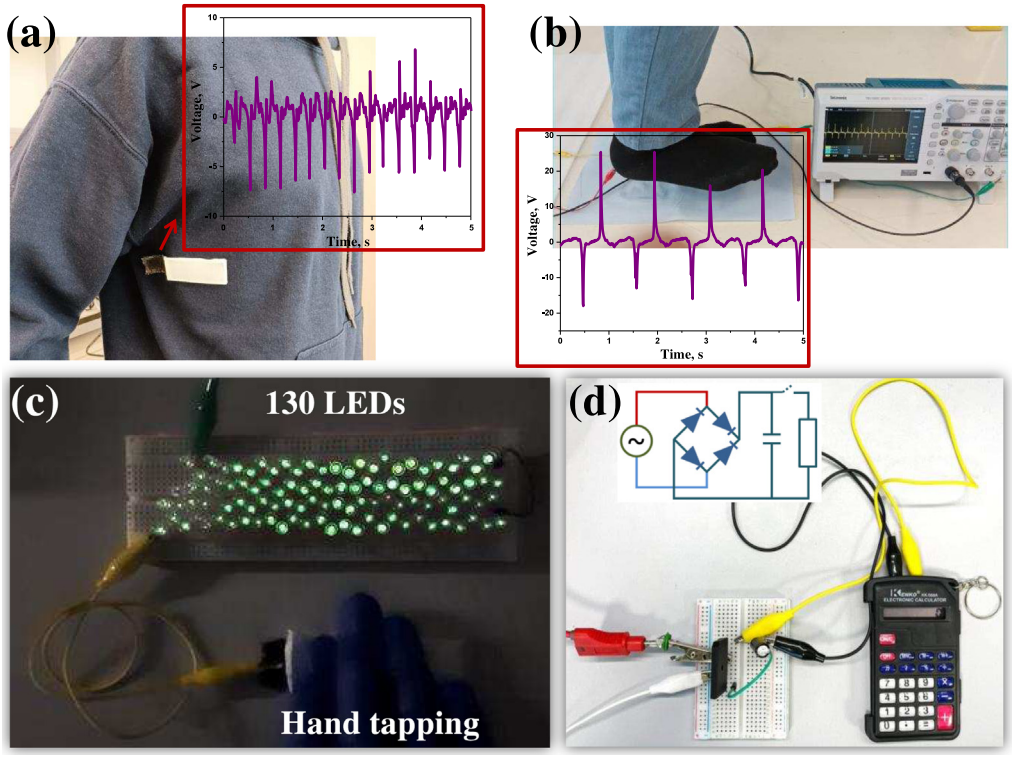

Fig. 7. Applications of CC@5%TiO_2-PDMS SETENG:(a) real-time energy scavenging under arm and (b) under foot heel, (c) powering 130 LEDs, (d) calculator working by a SETENG source through a 220-μF capacitor.

Table 1
Comparison of performances of SETENGs based on PDMS materials.

TENG material	Working mode	Performance	Ref.
PDMS-MXene	single-electrode mode	TENG provided a maximum V_{oc} of 170 V and I_{sc} of 20 μA cm^{-2}.	(He et al., 2020)
PDMS-Fe	single-electrode mode	The PDMS-Fe 10 wt% based TENG gives the highest V_{oc} of 70 V and I_{sc} of 250 nA.	(Seo et al., 2021)
Porous PDMS-Na_2CO_3	single-electrode mode	Na_2CO_3/PDMS TENG had V_{oc} of 125 V.	(Cui et al., 2018)
PDMS-Ti_2O	single-electrode mode	5 wt% Ti_2O NPs demonstrated V_{oc} and I_{sc} of 116 V and 1.42 μA.	This work

Funding

This work was supported by the research grants AP08052143 "Development of wearable self-charging power unit", AP14869428 "Mechanical energy harvesting system based on hybrid nanogenerators" from the Ministry of Education and Science of the Republic of Kazakhstan and 240919FD3914 "Self-Charging Rechargeable Lithium-ion Battery", Collaborative Research Program Grant no. 11022021CRP1513 from Nazarbayev University.

CRediT authorship contribution statement

Roman Kruchinin: Writing – review & editing, Investigation, Methodology. **Yerzhan Nurmakanov:** Writing – review & editing, Investigation, Methodology. **Galymzhan Nauryzbayev:** Writing – review & editing. **Desmond Adair:** Writing – review & editing. **Zhumabay Bakenov:** Writing – review & editing. **Gulnur Kalimuldina:** Conceptualization, Supervision, Writing – review & editing, Funding acquisition.

Declaration of competing interest

The authors declare that they have no known competing financial interests or personal relationships that could have appeared to influence the work reported in this paper.

Data availability

Data will be made available on request.

Appendix A. Supplementary data

Supplementary material related to this article can be found online at https://doi.org/10.1016/j.egyr.2022.11.049.

References

Ali, D., Yu, B., Duan, X., Yu, H., Zhu, M., 2017. Enhancement of output performance through post-poling technique on BaTiO3/PDMS-based triboelectric nanogenerator. Nanotechnology 28, 75203.
Cao, X., Jie, Y., Wang, N., Wang, Z.L., 2016. Triboelectric nanogenerators driven self-powered electrochemical processes for energy and environmental science. Adv. Energy Mater. 6, 1600665.
Chen, J., Wang, Z.L., 2017. Reviving vibration energy harvesting and self-powered sensing by a triboelectric nanogenerator. Joule 1, 480–521.
Cheng, G.-G., Jiang, S.-Y., Li, K., Zhang, Z.-Q., Wang, Y., Yuan, N.-Y., Ding, J.-N., Zhang, W., 2017. Effect of argon plasma treatment on the output performance of triboelectric nanogenerator. Appl. Surf. Sci. 412, 350–356.
Cui, C., Wang, Xingzhao, Yi, Z., Yang, B., Wang, Xiaolin, Chen, X., Liu, J., Yang, C., 2018. Flexible single-electrode triboelectric nanogenerator and body moving sensor based on porous Na2CO3/polydimethylsiloxane film. ACS Appl. Mater. Interfaces 10, 3652–3659.
Dharmasena, R.D.I.G., Silva, S.R.P., 2019. Towards optimized triboelectric nanogenerators. Nano Energy 62, 530–549.
Dudem, B., Bharat, L.K., Patnam, H., Mule, A.R., Yu, J.S., 2018. Enhancing the output performance of hybrid nanogenerators based on Al-doped BaTiO3 composite films: a self-powered utility system for portable electronics. J. Mater. Chem. A 6, 16101–16110.
Dudem, B., Mule, A.R., Patnam, H.R., Yu, J.S., 2019. Wearable and durable triboelectric nanogenerators via polyaniline coated cotton textiles as a movement sensor and self-powered system. Nano Energy 55, 305–315.
Fan, F.-R., Lin, L., Zhu, G., Wu, W., Zhang, R., Wang, Z.L., 2012a. Transparent triboelectric nanogenerators and self-powered pressure sensors based on micropatterned plastic films. Nano Lett. 12, 3109–3114.
Fan, F.-R., Tian, Z.-Q., Lin Wang, Z., 2012b. Flexible triboelectric generator. Nano Energy 1, 328–334.
Fang, Z., Chan, K.H., Lu, X., Tan, C.F., Ho, G.W., 2018. Surface texturing and dielectric property tuning toward boosting of triboelectric nanogenerator performance. J. Mater. Chem. A 6, 52–57.
He, W., Sohn, M., Rujun Ma, R., Kang, D.J., 2020. Flexible single-electrode triboelectric nanogenerators with MXene/PDMS composite film for biomechanical motion sensors. Nano Energy 78, 105383.
Jian, G., Meng, Q., Jiao, Y., Feng, L., Shao, H., Wang, F., Meng, F., 2021. Hybrid PDMS-TiO2-stainless steel textiles for triboelectric nanogenerators. Chem. Eng. J. 417, 127974.
Jin, T., Sun, Z., Li, L., Zhang, Q., Zhu, M., Zhang, Z., Yuan, G., Chen, T., Tian, Y., Hou, X., Lee, C., 2020. Triboelectric nanogenerator sensors for soft robotics aiming at digital twin applications. Nat. Commun. 11, 5381.
Kang, X., Pan, C., Chen, Y., Pu, X., 2020. Boosting performances of triboelectric nanogenerators by optimizing dielectric properties and thickness of electrification layer. RSC Adv. 10, 17752–17759.
Khandelwal, G., Maria Joseph Raj, N.P., Kim, S.-J., 2020. Triboelectric nanogenerator for healthcare and biomedical applications. Nano Today 33, 100882.
Khandelwal, G., Maria Joseph Raj, N.P., Kim, S.-J., 2021. Materials beyond conventional triboelectric series for fabrication and applications of triboelectric nanogenerators. Adv. Energy Mater. 11, 2101170.
Kim, M.P., Um, D.-S., Shin, Y.-E., Ko, H., 2021. High-performance triboelectric devices via dielectric polarization: A review. Nanoscale Res. Lett. 16 (35).
Luo, J., Wang, Z.L., 2020. Recent progress of triboelectric nanogenerators: From fundamental theory to practical applications. EcoMat 2, e12059.
McCarty, L.S., Whitesides, G.M., 2008. Electrostatic charging due to separation of ions at interfaces: Contact electrification of ionic electrets. Angew. Chem. Int. Ed. 47, 2188–2207.
Min, G., Xu, Y., Cochran, P., Gadegaard, N., Mulvihill, D.M., Dahiya, R., 2021. Origin of the contact force-dependent response of triboelectric nanogenerators. Nano Energy 83, 105829.
Mishra, A., Shetti, N.P., Basu, S., Raghava Reddy, K., Aminabhavi, T.M., 2019. Carbon cloth-based hybrid materials as flexible electrochemical supercapacitors. ChemElectroChem 6, 5771–5786.
Mule, A.R., Dudem, B., Patnam, H., Graham, S.A., Yu, J.S., 2019. Wearable single-electrode-mode triboelectric nanogenerator via conductive polymer-coated textiles for self-power electronics. ACS Sustain. Chem. Eng. 7, 16450–16458.
Nie, J., Chen, X., Wang, Z.L., 2019. Electrically responsive materials and devices directly driven by the high voltage of triboelectric nanogenerators. Adv. Funct. Mater. 29, 1806351.
Niu, S., Liu, Y., Wang, S., Lin, L., Zhou, Y.S., Hu, Y., Wang, Z.L., 2014. Theoretical investigation and structural optimization of single-electrode triboelectric nanogenerators. Adv. Funct. Mater. 24, 3332–3340.
Niu, S., Wang, S., Lin, L., Liu, Y., Zhou, Y.S., Hu, Y., Wang, Z.L., 2013. Theoretical study of contact-mode triboelectric nanogenerators as an effective power source. Energy Environ. Sci. 6, 3576–3583.
Nurmakanov, Y., Kalimuldina, G., Nauryzbayev, G., Adair, D., Bakenov, Z., 2021. Structural and chemical modifications towards high-performance of triboelectric nanogenerators. Nanoscale Res. Lett. 16, 122.
Park, H.-W., Huynh, N.D., Kim, W., Hwang, H.J., Hong, H., Choi, K., Song, A., Chung, K.-B., Choi, D., 2018. Effects of embedded TiO2-x nanoparticles on triboelectric nanogenerator performance. Micromachines 9, 407.
Qian, Y., Sohn, M., He, W., Park, H., Subramanian, K.R.V., Kang, D.J., 2020. A high-output flexible triboelectric nanogenerator based on polydimethylsiloxane/three-dimensional bilayer graphene/carbon cloth composites. J. Mater. Chem. A 8, 17150–17155.
Seo, J., Hajra, S., Sahu, M., Kim, H.J., 2021. Effect of cilia microstructure and ion injection upon single-electrode triboelectric nanogenerator for effective energy harvesting. Mater. Lett. 304, 130674.
Shi, Q., Sun, Z., Zhang, Z., Lee, C., 2021. Triboelectric nanogenerators and hybridized systems for enabling next-generation IoT applications. Research 2021, 6849171.

Shi, H., Wen, G., Nie, Y., Zhang, G., Duan, H., 2020. Flexible 3D carbon cloth as a high-performing electrode for energy storage and conversion. Nanoscale 12, 5261–5285.
Tantraviwat, D., Ngamyingyoud, M., Sripumkhai, W., Pattamang, P., Rujijanagul, G., Inceesungvorn, B., 2021. Tuning the dielectric constant and surface engineering of a BaTiO3/Porous PDMS composite film for enhanced triboelectric nanogenerator output performance. ACS Omega 6, 29765–29773.
Wang, Z.L., 2013. Triboelectric nanogenerators as new energy technology for self-powered systems and as active mechanical and chemical sensors. ACS Nano 7, 9533–9557.
Wang, Z.L., 2014. Triboelectric nanogenerators as new energy technology and self-powered sensors – principles, problems and perspectives. Faraday Discuss 176, 447–458.
Wang, Z.L., Lin, L., Chen, J., Niu, S., Zi, Y., 2016. In: Wang, Z.L., Lin, L., Chen, J., Niu, S., Zi, Y. (Eds.), Triboelectric Nanogenerator: Single-Electrode Mode BT - Triboelectric Nanogenerators. Springer International Publishing, Cham, pp. 91–107.
Wang, S., Lin, L., Wang, Z.L., 2015. Triboelectric nanogenerators as self-powered active sensors. Nano Energy 11, 436–462.
Wang, S., Lin, L., Xie, Y., Jing, Q., Niu, S., Wang, Z.L., 2013. Sliding-triboelectric nanogenerators based on in-plane charge-separation mechanism. Nano Lett. 13, 2226–2233.
Wang, Y., Yang, Y., Wang, Z.L., 2017. Triboelectric nanogenerators as flexible power sources. Npj Flex. Electron. 1 (10).
Xia, K., Wu, D., Fu, J., Hoque, N.A., Ye, Y., Xu, Z., 2020. A high-output triboelectric nanogenerator based on nickel–copper bimetallic hydroxide nanowrinkles for self-powered wearable electronics. J. Mater. Chem. A 8, 25995–26003.
Xie, L., Chen, X., Wen, Z., Yang, Y., Shi, J., Chen, C., Peng, M., Liu, Y., Sun, X., 2019. Spiral steel wire based fiber-shaped stretchable and tailorable triboelectric nanogenerator for wearable power source and active gesture sensor. Nano-Micro Lett. 11, 39.
Zhang, X.-S., Han, M.-D., Wang, R.-X., Meng, B., Zhu, F.-Y., Sun, X.-M., Hu, W., Wang, W., Li, Z.-H., Zhang, H.-X., 2014. High-performance triboelectric nanogenerator with enhanced energy density based on single-step fluorocarbon plasma treatment. Nano Energy 4, 123–131.
Zhang, R., Olin, H., 2020. Material choices for triboelectric nanogenerators: A critical review. EcoMat 2, e12062.
Zhang, C., Wang, Z.L., 2016. Tribotronics—A new field by coupling triboelectricity and semiconductor. Nano Today 11, 521–536.
Zhou, M., Al-Furjan, M.S.H., Zou, J., Liu, W., 2018. A review on heat and mechanical energy harvesting from human – principles, prototypes and perspectives. Renew. Sustain. Energy Rev. 82, 3582–3609.
Zhou, Y., Deng, W., Xu, J., Chen, J., 2020. Engineering materials at the nanoscale for triboelectric nanogenerators. Cell Rep. Phys. Sci. 1, 100142.
Zhou, Q., Kim, J.-N., Han, K.-W., Oh, S.-W., Umrao, S., Chae, E.J., Oh, I.-K., 2019. Integrated dielectric-electrode layer for triboelectric nanogenerator based on Cu nanowire-mesh hybrid electrode. Nano Energy 59, 120–128.